

1 Joint inference of species histories and gene flow

2
3
4 Nicola F. Müller^{a,b,c,1}, Huw A. Ogilvie^d, Chi Zhang^{e,f}, Michael C. Fontaine^{g,h}, Jorge E. Amaya-Romero^{g,h},
5 Alexei J. Drummondⁱ and Tanja Stadler^{b,c}

6
7
8 ^a Fred Hutchinson Cancer Research Center, Vaccine and Infectious Disease Division, 98109 Seattle, USA

9 ^b ETH Zürich, Department of Biosystems Science and Engineering, 4058 Basel, Switzerland

10 ^c Swiss Institute of Bioinformatics (SIB), Switzerland

11 ^d Department of Computer Science, Rice University, Houston TX, USA

12 ^e Key Laboratory of Vertebrate Evolution and Human Origins, Institute of Vertebrate Paleontology and Paleoanthropology, Chinese
13 Academy of Sciences, Beijing 100044, China

14 ^f Center for Excellence in Life and Paleoenvironment, Chinese Academy of Sciences, Beijing 100044, China

15 ^g Laboratoire MIVEGEC (Université de Montpellier, UMR CNRS 5290, IRD 229) et Centre de Recherche en Ecologie et Evolution de la
16 Santé (CREES), Centre IRD de Montpellier, Montpellier, France

17 ^h Groningen Institute for Evolutionary Life Sciences (GELIFES), University of Groningen, PO Box 11103 CC, Groningen, The Netherlands

18
19 ⁱ Centre for Computational Evolution, University of Auckland, New Zealand

20 ¹Corresponding author

21 **Abstract:** When populations become isolated, members of these populations can diverge genetically over
22 time. This leads to genetic differences between these populations that increase over time if the isolation persists.
23 This process can be counteracted by gene flow, i.e. when genes are exchanged between populations. In order to
24 study the speciation processes when gene flow is present, isolation-with-migration methods have been developed.
25 These methods typically assume that the ranked topology of the species history is already known. However,
26 this is often not the case and the species tree is therefore of interest itself. For the inference of species trees, it
27 is in turn often necessary to assume that there is no gene flow between co-existing species. This assumption,
28 however, can lead to wrongly inferred speciation times and species tree topologies. We here introduce a new
29 method that allows inference of the species tree while explicitly modelling the flow of genes between coexisting
30 species. By using Markov chain Monte Carlo sampling, we co-infer the species tree alongside evolutionary
31 parameters of interest. By using simulations, we show that our newly introduced approach is able to reliably
32 infer the species trees and parameters of the isolation-with-migration model from genetic sequence data. We then
33 use this approach to infer the species history of the mosquitoes from the *Anopheles gambiae* species complex.
34 Accounting for gene flow when inferring the species history suggests a slightly different speciation order and
35 gene flow than previously suggested.

36 Introduction

37 Populations can diverge genetically and become separated over time, due to geography or other factors. Gene flow
38 after populations become genetically isolated can counteract this process (Sousa and Hey, 2013). These events are
39 captured in the genome of sampled individuals of those species. In turn, the genetic sequences of sampled species
40 allow us to draw inferences about their common history (the species phylogeny) by modelling the speciation
41 process. To reconstruct the speciation process from genetic sequence data, the multispecies coalescent model
42 (MSC) can be used (Rannala and Yang, 2003; Liu *et al.*, 2009; Heled and Drummond, 2010). This allows for the
43 reconstruction of the species tree while accounting for discordance between gene trees due to incomplete lineage
44 sorting. Gene flow after populations become genetically isolated can counteract this process of divergence (Sousa
45 and Hey, 2013), and if not accounted for, this can lead to biased inferences about the ancestral history of the
46 species (Leaché *et al.*, 2014). To account for gene flow after speciation, isolation-with-migration (IM) models
47 have been developed (Nielsen and Wakeley, 2001; Hey and Nielsen, 2004; Wilkinson-Herbots, 2008) (see also
48 Sousa and Hey, 2013, for review). Initial Bayesian implementations of the IM model were applicable to only
49 two populations. Further, they could suffer from poor Markov chain Monte Carlo (MCMC) convergence due to
50 an extremely diffuse parameter space (Nielsen and Wakeley, 2001; Hey and Nielsen, 2004).

51 This difficulty was partly overcome by analytically integrating out some model parameters (population sizes
52 and migration rates) to sample from the posterior distribution of gene trees and speciation times. The gene trees
53 and speciation times are then used to estimate the evolutionary parameters and the effective population sizes
54 and rates of gene flow (Hey and Nielsen, 2007). This approach was later extended to deal with more than two
55 populations (Hey, 2010). All of these methods required the species tree topology and the ordering of speciation
56 times to be known *a priori*.

57 One of the challenges that restricts joint inference of the species tree and rates of gene flow is that, over
58 the course of an MCMC, different species can co-exist. This means gene flow can happen between different co-
59 existing species at different stages of the MCMC. When operating on the species tree such that the co-existing
60 species change, some of the possible routes of gene flow disappear and some newly appear. At the same time,
61 this means that the migration history of a gene tree, i.e. an explicit sequence of migration events, is possibly
62 no longer valid after a new species tree is proposed. Operating on the species tree is therefore particularly
63 challenging if the migration history of each gene tree has to be explicitly considered as well. In Hey *et al.* (2018),
64 this challenge was overcome by using a clever mapping of migration events between extant species to ancestral
65 species using what is called a hidden genealogy. This means that for any ranked species history, migration
66 histories are always defined.

67 Having to infer migration histories can lead to computational issues in the related structured coalescent
68 model (De Maio *et al.*, 2015; Müller *et al.*, 2017). Alternatively, inferring migration histories could be avoided
69 altogether.

70 Here, we introduce a novel isolation-with-migration model (AIM) that allows joint inference of the species
71 tree with rates of gene flow and effective population sizes that avoids the sampling of migration histories. We do
72 so by extending the marginal approximation of the structured coalescent (Müller *et al.*, 2017) to the isolation-
73 with-migration model. Modelling the movement of lineages between speciation events as a structured coalescent
74 process allows us to evaluate the probability of a gene tree given a species tree, a set of rates of gene flow and
75 effective population sizes. The probability of a gene tree given any species tree and set effective population sizes
76 and rates of gene flow can always be calculated using this framework. Using MCMC sampling, we can then
77 operate on the species tree topology, divergence times, gene trees, rates of gene flow and effective population
78 sizes for extinct and extant species. We implemented this approach as an update to StarBEAST2 (Ogilvie *et al.*,
79 2017), which is available as a package for the phylogenetic software platform BEAST2 (Bouckaert *et al.*, 2014,
80 2019).

81 By using simulations, we show that the AIM model is able to infer rates of gene flow (which are equivalent
82 to migration rates in the structured coalescent model), effective population sizes and species trees reliably from
83 molecular sequences directly. In contrast to AIM, the MSC can strongly support wrong species tree topologies

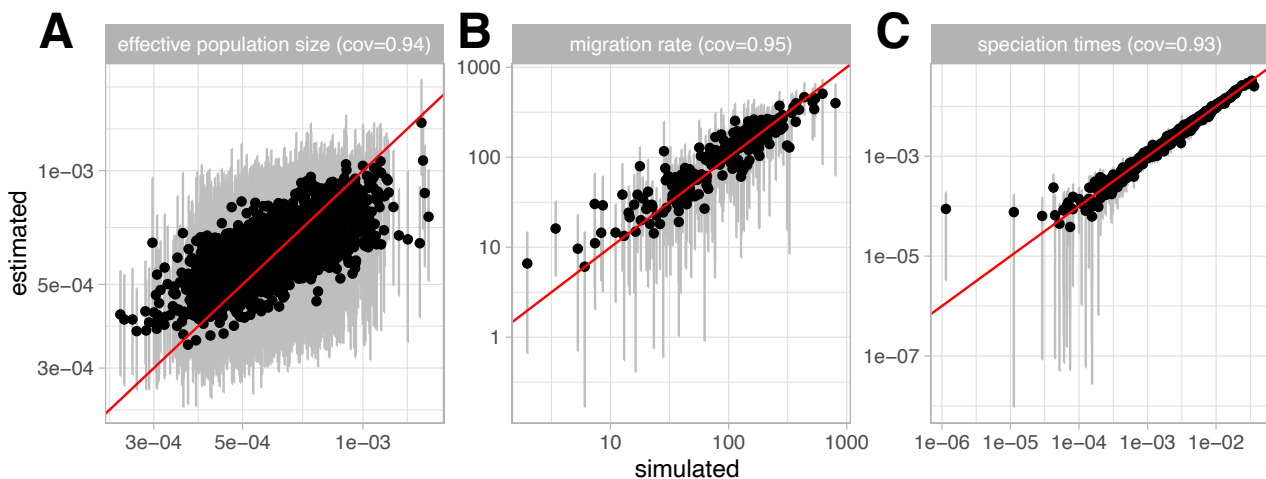


Figure 1: **Inference of effective population sizes, migration rates and speciation times.** **A** Here we compare estimated effective population sizes on the y-axis to the true simulated effective population sizes on the x-axis. The grey bar represent the 95% highest posterior density interval. **B** Comparison between estimated and simulated migration rates conditional on there being gene flow. The estimated support for gene flow is shown separately in figure 2. **C** Estimated versus simulated speciation times.

84 and systematically underestimate speciation times.

85 We then apply AIM to jointly infer the species trees and the rate of gene flow between individual *anopheles*
86 species from the *Anopheles gambiae* species complex (AGC) (Fontaine *et al.*, 2015). The AGC consists of at
87 least eight distinct species that are morphologically indistinguishable (Davidson, 1962; White *et al.*, 2011). Three
88 of these species are amongst the worlds most important malaria vectors (*An. gambiae*, *An. coluzzii*, and *An.*
89 *arabiensis*). Interestingly, this species complex has become a flagship example of reticulated evolution (Mallet
90 *et al.*, 2016; Clark and Messer, 2015). Deciphering the species tree in the AGC remained a challenge for decades
91 due to the confounding processes of incomplete lineage sorting and gene flow that blurred the species tree. The
92 X chromosome and the autosome of these *anopheles* species have been described to code for vastly different
93 species tree topologies (Fontaine *et al.*, 2015) and only 2% of the genome, mostly located on the X chromosome,
94 has been suggested to reflect the true species order (Fontaine *et al.*, 2015; Thawornwattana *et al.*, 2018). This
95 dataset has been previously analysed using different methods. Fontaine *et al.* (2015) inferred the speciation
96 history directly from the gene trees themselves, while Thawornwattana *et al.* (2018) inferred the speciation
97 history by using a multi-species coalescent approach implemented in BPP (Yang, 2015a).

98 Results

99 Inference of the species tree from genetic sequences

100 We first test if AIM is able to infer the true species tree, rates of gene flow and effective population sizes of extant
101 and extinct species. To do so, we first simulated 1000 species trees with 4 taxa under the Yule model (Yule,
102 1925) with a speciation rate randomly sampled from a lognormal distribution with mean=100 and $\sigma=0.1$. The
103 narrow distribution around the speciation rate is chosen such there are no issues arising from migration rates
104 or effective population sizes being too high or low relative to the species tree.

105 For each of those 1000 randomly sampled species trees, we next sampled at random the effective population

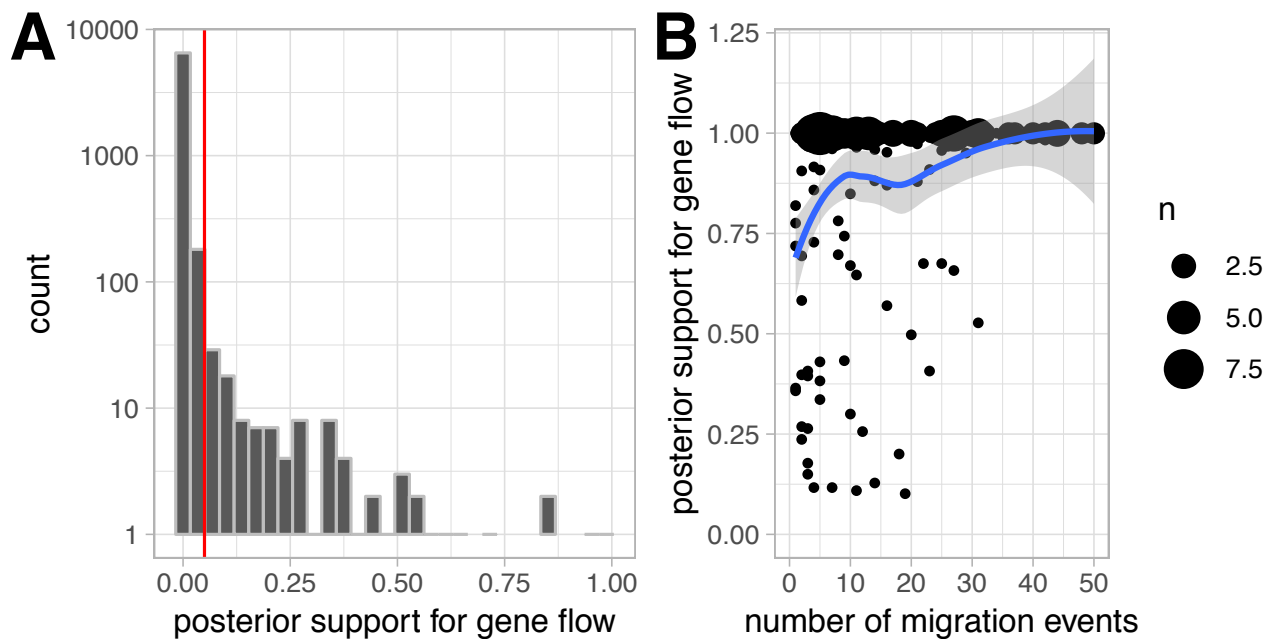


Figure 2: **Posterior support for gene flow.** **A** Distribution of the support of gene flow between species for which there was no gene flow in the simulations. The x-axis shows the support for gene flow and the y-axis shows the amount of times that posterior support was observed in log scale. The red line shows the prior support for gene flow. **B** Posterior support for gene flow on the y-axis versus the number of migration events between the two species on the x-axis. The curve is a mean estimate for the posterior support of gene flow for different numbers of migration events. The mean estimates are calculated using a loess regression between the number of migration events and the posterior support for gene flow.

106 sizes of each species from a lognormal distribution with mean=0.0025 and standard deviation=0.25. Between
107 each co-existing species, we randomly sampled if there is on-going gene flow from a binomial distribution with
108 5% probability on there being gene flow. This put an approximately 40% probability of there not being any
109 gene flow in the simulated datasets, meaning that these simulations include datasets with and without gene
110 flow. If there was gene flow, we sampled the forward in time migration rate from an exponential distribution
111 with mean=100. Additionally, we say that the rate of each lineage having originated from a different species
112 is at most the inverse time of co-existence between two species. Without that constraint, we would allow for
113 scenarios where speciation events are entirely unobserved.

114 For each of the 1000 simulated species trees, effective population sizes and migration rates, we simulated
115 50 gene trees using MCcoal (Yang, 2015b). Each of the four species had 2 sampled individuals. For each of the
116 gene trees, we next simulated genetic sequences using the HKY model with a transition/transversion ratio of 3
117 and assuming a random relative evolutionary rate scaler drawn from an exponential distribution with mean=1
118 using SeqGen (Rambaut and Grassly, 1997).

119 We next used AIM to jointly infer the species tree, rates of gene flow, and effective population sizes of
120 all extant and ancestral species and evolutionary rates from the simulated sequences. For each rate of gene
121 flow between two co-existing species, we estimate the support for this rate to be non zero using the BSSVS
122 approach (Lemey et al., 2009a). As shown in figure 1, effective population sizes, migration rates and speciation
123 times are inferred reliably. As expected, the 95% highest posterior density (HPD) intervals contain the true

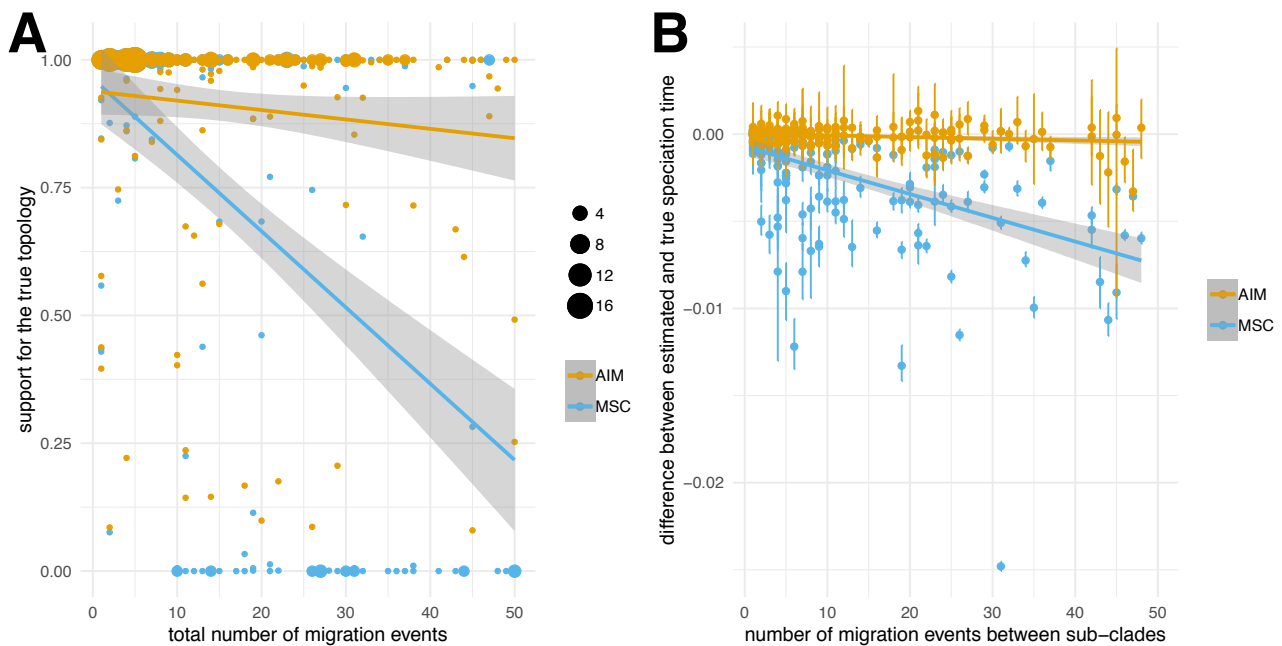


Figure 3: **Comparison of species tree and speciation time inference using AIM and MSC.** **A** Posterior support for the true species tree topology inferred using the approximate isolation with migration (AIM) model and the multispecies coalescent (MSC). The curve denote the mean support for the true species tree topology calculated using a linear regression between the total number of migration events and the support for the true topology. **B** Comparison between the 95% highest posterior density intervals of speciation times between AIM and MSC. As shown in figure 1C, AIM infers the true speciation times well. The multispecies coalescent is biased towards an underestimation of the speciation time.

124 values under which the simulation was performed in around 95% of all cases.

125 We next study the ability of AIM to detect gene flow. To do so, we first computed the distribution of
 126 posterior support for gene flow between species for which no gene flow was present in the simulations. As shown
 127 in figure 2a, AIM is able to reject gene flow when there is none present. Second, when there are migration events
 128 between species, as shown in figure 2b, the model is mostly able to infer that gene flow occurred. This is the
 129 case except for a few simulations, where the support for gene flow is lower, but still greater than the prior for
 130 gene flow.

131 Lastly, we compare the inference of species tree topologies and speciation times between accounting for gene
 132 flow (AIM) and not accounting for it (MSC). To do so, we analysed the same simulated datasets using StarBeast2
 133 where we jointly infer the species history, effective population sizes of each species as well as all evolutionary
 134 parameters. StarBeast2 implements the multispecies coalescent model in BEAST2. For most simulated datasets,
 135 both methods infer the species tree topology well, with AIM inferring higher posterior support for the true
 136 topology (see figure S1A). The estimates of speciation times are largely consistent between the two methods
 137 (see figure S1B).

138 Between most species, however, there was no gene flow in the simulations. To see when there are differences
 139 between the two approaches, we next look at the support for the true species tree topology depending on
 140 the overall number of migration events (see figure 3A). With more and more migration events, the support
 141 for the true species tree topology decreases using the multi-species coalescent. Using AIM, the support for

142 the true species tree topology is largely independent of the total number of migration events (see figure 3A).
143 Figure 3B shows the estimated minus the true speciation times using the two approaches. These results are shown
144 depending on how many migration events happened between the two clades below each speciation event. The
145 more migration events there were between these two clades, the stronger the underestimation of the speciation
146 time becomes. In other words, if there are migration events between two clades, the multi-species coalescent
147 infers speciation events to have occurred closer to the present. The speciation time estimates using AIM are
148 largely unaffected by this. This observation is consistent with biases in inference of speciation times observed
149 previously (Leaché et al., 2014).

150 Resolving the evolutionary history of *Anopheles gambiae* complex

151 Next, we used (AIM) to study the species history of the *An. gambiae* species complex (AGC). Previous stud-
152 ies Fontaine et al. (2015); Thawornwattana et al. (2018) showed that different regions of the genomes of the
153 AGC code for different topologies, especially with respect to the branching of *An. arabiensis*. Most of the
154 X-chromosome (i.e. the Xag inversion) was shown to be indicative of the species branching order, where *An.*
155 *arabiensis* cluster with *An. quadriannulatus* (Fontaine et al., 2015). In contrast, the autosomes were shown to
156 be strongly impacted by introgressions between *An. arabiensis* and *An. gambiae* or *An. coluzzii* (Fontaine et al.,
157 2015). Here, we assessed the ability of AIM to reconstruct the species history of the AGC in two ways, namely
158 analyzing only the x-chromosome and analyzing both the x-chromosome and chromosome 3. We first split the
159 chromosome into loci of approximately 1000 base pairs.

160 After removing all loci which had variable sites on more than 50% of all positions, we randomly sampled 200
161 loci along the X chromosome. In order to control for sensitivity due to this random sub-sampling, we repeated
162 this step 3 times. We then jointly inferred the species history and the support for gene flow between individual
163 species from these regions. We assumed the different regions to evolve according to an HKY+ Γ_4 model with
164 a transition/transversion rate that we estimated for each region individually, while fixing the base frequencies
165 to the observed frequencies. We further allowed each region to have a different relative evolutionary rate. Since
166 we only have loci from one individual per species, we further assumed that the effective population size of all
167 extant species was the same. The reason is that with having only one sampled individual per species, coalescent
168 events in extant species can only occur when there is gene flow to extant species. This means that there are
169 only very few or no coalescent events in a species to inform effective population sizes in extant species.

170 Figure 4 shows the inferred evolutionary history of 8 anopheles species, including the two outgroup species
171 (*An. christyi* and *An. epiroticus*), averaged over the 3 random subsets. Using the AIM model, we inferred that
172 *An. merus* had its most recent speciation event with the common ancestor of *An. coluzzii* and *An. gambiae*.
173 Fontaine et al. (2015) showed that the bottom of the species tree was poorly resolved using classic phylogenetic
174 approaches due primarily to incomplete lineage sorting. In contrast, Thawornwattana et al. (2018) inferred
175 that *An. merus* was the first species to split from the rest of the *An. gambiae* species complex using the MSC
176 and 100 loci. The branching order for the rest of the tree was consistent with both Fontaine et al. (2015)
177 and Thawornwattana et al. (2018).

178 We inferred the common ancestor of all species, expect the outgroups to be about 0.4 Million years ago
179 assuming the same evolutionary rate of $3.08 * 10^{-8}$ per year as in Keightley et al. (2014) and Thawornwattana
180 et al. (2018) for non-coding loci. We estimate the isolation events of populations to have happened earlier
181 than the estimates of speciation events in Thawornwattana et al. (2018). Since we, however, sub-sample loci
182 depending on how much variation they have, the speciation time estimates might not be directly comparable.
183 We, for example, also infer a slightly more distant divergence time with *An. christyi* of approximately 0.1
184 compared to 0.08 substitutions per site in Thawornwattana et al. (2018). If we assume that this difference is
185 due to different sub-sampling of loci, our inferred common ancestor time of the *An. gambiae* species complex is
186 consistent with Thawornwattana et al. (2018).

187 Jointly with the speciation history, we inferred the presence of gene flow between any co-existing species.
188 Gene flow is indicated by arrows between two co-existing species. Arrows are plotted for gene flow between

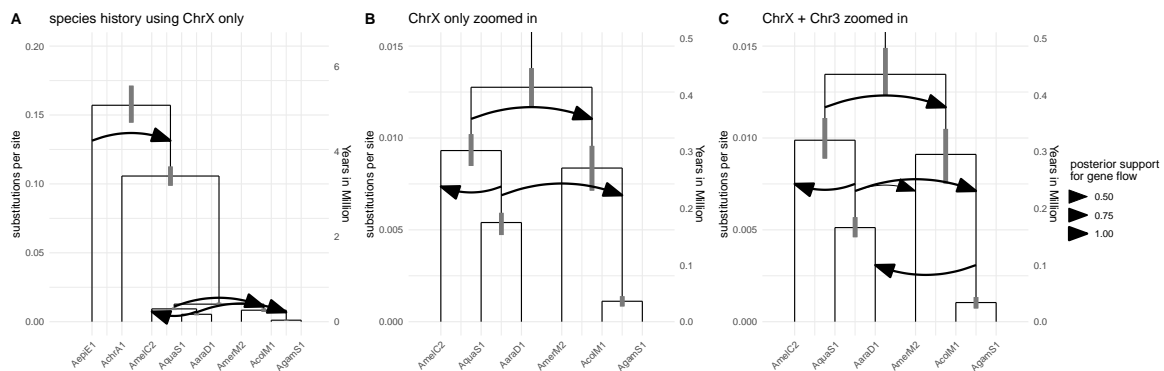


Figure 4: Inferred species evolutionary history of the *An. gambiae* complex. The inferred species history of anopheles is shown in units of substitutions per site averaged over all 3 random subsets of loci from either only the X chromosome (ChrX) or from the X chromosome and chromosome 3 (ChrX + Chr3). The node heights are the median inferred speciation times. The grey bars show the 95% highest posterior density intervals for speciation times. The heights are given in substitutions per site. The cutoff for an arrow to be plotted is support for gene flow with a posterior support of at least 0.5. **A** Inferred species history for all 8 anopheles species including the two outgroups *An. christyi* and *An. epiroticus*, with support for ancestral gene flow between them. This analysis was done by averaging the results over 3 random subsets of 200 loci from the X chromosome. **B** Inferred species history of the same anopheles species but zoomed into the *An. gambiae* species complex. **C** Inferred species history of the anopheles species averaged over 3 random subsets of 200 loci from the X chromosome and chromosome 3. Each of the 200 loci had a 75% chance to be from the X-chromosome and a 12.5% chance to be from the left or right arm of chromosome 3. The inference was done using all 8 species, but the results are zoomed into the *An. gambiae* species complex.

189 species with a posterior support of at least 0.5. We find support for gene flow between *An. epiroticus* and the
 190 common ancestor of all other species in all random subsets (see figures 4A & S4).

191 Over all datasets and different number of samples, we infer gene flow from the ancestral species of *An.*
 192 *arabiensis* and *An. quadriannulatus* to the ancestral species of *An. coluzzii* and *An. gambiae* (see figures 4B
 193 & S5).

194 The rates of gene flow were estimated using only loci from the X chromosome, where there is little information
 195 about gene flow (Fontaine *et al.*, 2015; Thawornwattana *et al.*, 2018). In fact, most of the information about
 196 gene flow has been reported to lie on the autosomes (Fontaine *et al.*, 2015). To test how the inference changes
 197 when including loci from the autosomes, we next compiled 3 random datasets of 200 loci with each loci having a
 198 75% chance of being from the X chromosome and a 0.25 and loci from chromosome 3. The higher probability of
 199 including loci from the X chromosome is chosen such that there is still enough information about the species tree
 200 in the dataset. We then jointly inferred the species tree and gene flow using the same priors and evolutionary
 201 models as before for each dataset.

202 We find support for gene flow between the same co-existing species when including loci from chromosome 3
 203 (see figures 4C & S5).

204 For all three random subsets, we now find support for gene flow from the ancestral species of *An. coluzzii*
 205 and *An. gambiae* to *An. arabiensis*, which is consistent with Fontaine *et al.* (2015) (see figure S5). This inferred
 206 directionality of gene flow is consistent with Fontaine *et al.* (2015) and Thawornwattana *et al.* (2018). In 2 of
 207 the 3 random subsets, we also find support for gene flow between between *An. merus* and the ancestral species
 208 of *An. quadriannulatus* and *An. arabiensis*, but not between *An. merus* and *An. quadriannulatus* as in Fontaine
 209 *et al.* (2015).

210 Discussion

211 The AIM model and its implementation introduced here is able to jointly estimate the species tree topology and
212 times, effective population sizes, and rates of gene flow between species, from multi locus molecular sequence
213 data. These parameters are relevant to many biological systems. Our approach is implemented in a new version
214 of an open source package (StarBEAST2) which is an add-on to the phylogenetics software platform (BEAST2).
215 This means that users of AIM can take advantage of the flexibility of BEAST2, including the large number of
216 available molecular clock models and substitution models.

217 Using simulations, we demonstrate the validity of our approach as well as the problems that can occur
218 when gene flow is not accounted for. The species tree topologies and node heights are inferred accurately in
219 all scenarios we simulated. Not accounting for gene flow can lead to underestimated speciation times as well
220 as incorrect species tree topologies. This is consistent with previous observations (Leaché *et al.*, 2014). The
221 estimates of rates of gene flow are unbiased but inferring support for gene flow can be complex when only a few
222 gene flow events in the datasets are captured in the gene trees.

223 When analysing the species history from random loci of the X chromosome of eight *Anopheles* species, we
224 inferred a different speciation order compared to previous results using the multi-species coalescent (Thaworn-
225 wattana *et al.*, 2018). In particular, we estimate *An. merus* to attach to the common ancestor of *An. coluzzii* and
226 *An. gambia*, whereas Thawornwattana *et al.* (2018) inferred *An. merus* to be an outgroup to the other species
227 of the ACG complex. This differences can be explained by what the different models consider a speciation event.
228 In the multi-species coalescent, a speciation event is more or less considered the last time genes were exchanged
229 between populations, whereas the isolation-with-migration model considers the initial isolation of populations
230 to be a speciation event.

231 Jointly with the species history, we inferred gene flow between co-existing species. When only using loci
232 from the X chromosome, we did not find support for gene flow from *An. arabiensis* to the ancestral species of
233 *An. coluzzii* and *An. gambia* as found previously (Fontaine *et al.*, 2015; Thawornwattana *et al.*, 2018). This is
234 expected since genes carrying information about gene flow between those two species are mostly located on the
235 autosomes. Instead, however, we found support for gene flow between the ancestral species of *An. arabiensis*
236 and *An. quadriannulatus* and *An. coluzzii* and *An. gambia*.

237 When including genes from chromosome 3, we find support for gene flow from *An. arabiensis* to the ancestral
238 species of *An. coluzzii* and *An. gambia* Additionally, we find support for gene flow from the ancestral species
239 of *An. arabiensis* and *An. quadriannulatus* to *An. merus*, but not from *An. quadriannulatus* directly. Random
240 selection of loci could however miss some of the information about gene flow. It remains to be seen if sub-
241 sampling strategies that perform a weighted selection of loci to better reflect the information content across the
242 full chromosome would allow us to better infer gene flow. Additionally, using more loci could allow us to better
243 capture more rare gene flow events. This may, however, require better Markov Chain Monte Carlo operators
244 that are able to more efficiently explore the posterior probability space. In particular, we currently do not utilize
245 Markov Chain Monte Carlo operators that jointly propose changes to gene trees and rates of gene flow between
246 co-existing species. Adding such might substantially increase the amount of loci that can be used for inferences.

247 The implementation of AIM as part of StarBeast2 further allows to include additional sources of data
248 such as fossil data to infer the species tree (Ogilvie *et al.*, 2018) using the Fossilize-Birth-Death model frame-
249 work (Stadler, 2010). Additionally, since the underlying structured coalescent theory has been developed ex-
250 plicitly for serially sampled data (Müller *et al.*, 2017, 2018), accounting for ancient DNA will be possible in the
251 future. This will mostly mainly require adapting the implementation to allow loci to be sampled through time,
252 analogue to, for example, pathogen sequence data. Additional Potential extensions to the model could only
253 allow migration to occur for a defined period of time after speciation (Wilkinson-Herbots, 2012). Alternatively,
254 additional information, such as about the overlap of habitats of species, could be used to inform gene flow
255 between species in a generalized linear model framework (Lemey *et al.*, 2014; Mueller *et al.*, 2018).

256 Materials and Methods

257 Calculation of the probability of a gene tree under the approximate isolation-with- 258 migration model

To calculate the probability of a gene tree under the approximate isolation-with-migration (AIM) model, the following probability has to be calculated:

$$P(T_G|T_S, S, \mathcal{M}, \mathcal{N})$$

259 with T_G being the gene tree, T_S being the species tree, S being the species to which each sampled individual
260 belongs and \mathcal{M} and \mathcal{N} being the set of migration rates and effective population sizes. To allow for multi-locus
261 data, we assume that each locus evolved independently from the same isolation-with-migration process.

262 The location of a gene over time

Isolation-with-migration models are closely related to the structured coalescent process. These models generally require the state or location of every single lineage to be inferred backwards in time. A recently introduced approximation to the structured coalescent avoids this by formally integrating over every possible history (Müller et al., 2017). For each given gene tree T_G , we calculate the probability of a lineage L_i at time t being in a particular state a (i.e. the gene being in a particular species a), $P_t(L_i = a|T_G)$. Between speciation on species trees and coalescent events on gene trees, this probability can be described via differential equations as described in Müller et al. (2018) eqn. 1:

$$\begin{aligned} \frac{d}{dt}P_t(L_i = a|T_G) = & \sum_{b=1}^s \left(m_{ba}P_t(L_i = b|T_G) - m_{ab}P_t(L_i = a|T_G) \right) \\ & + P_t(L_i = a|T_G) \sum_{b=1}^s \frac{1}{N_{e_b}} P_t(L_i = b|T_G) \sum_{\substack{k=1 \\ k \neq i}}^n P_t(L_k = b|T_G) \\ & - P_t(L_i = a|T_G) \frac{1}{N_{e_a}} \sum_{\substack{k=1 \\ k \neq i}}^n P_t(L_k = a|T_G) \quad (1) \end{aligned}$$

263 m_{ba} describes the backwards in time rate at which migration events from species b to a happen and N_{e_a} is the
264 effective population size of species a and s denotes the number of species. At a coalescent event between lineage
265 i and j , the probability of the parent lineage can be calculated using the following equation (14, page 2979):

$$P_t(L_{parent} = a, T_G) = \frac{1}{N_{e_a}} P_t(L_i = a|T_G) P_t(L_j = a|T_G) P_t(T_G) \quad (2)$$

266 Then we can proceed solving eqn. 1 again backward in time with the initial value $P_t(L_{parent} = a|T_G) =$
267 $P_t(L_{parent} = a, T_G)/P_t(T_G)$.

268 The location of a gene prior to a speciation event

269 $P(T_G|T_S, S, \mathcal{M}, \mathcal{N})$ can be calculated similar to the probability of a tree under the structured coalescent. Between
270 speciation events, $P(T_G|T_S, S, \mathcal{M}, \mathcal{N})$ is updated as shown in the previous section. The backwards in time
271 analogue to a speciation event is the combination of two species. If species a and species b have parent species
272 c , the probability of each remaining gene i being in species c can be calculated as follows:

$$P_t(L_i = c|T_G) = P_t(L_i = a|T_G) + P_t(L_i = b|T_G) \quad (3)$$

273 Starting from the present and going back in time, $P_t(L_i = a|T_G)$ can now be calculated using equations 1 and 2
274 between speciation events and using equation 3 at speciation events up to the root, $P_{root}(L_i = rootspecies|T_G)$.

275 Prior assumption of rates of gene flow

276 We assume the rates of gene flow to be constant over time and we allow them to be either forward or backward
277 in time. Backwards in time rates $m_{b,a}^b$ denote the probability of a lineage being in species b to have originated
278 from species a . The forwards in time rates $m_{a,b}^f$ denote the probability of an individual being in species a to
279 migrate to species b . This rate is not directly accessible in a coalescent framework, but can be approximated as:

$$280 \quad m_{b,a}^b \approx \frac{N_{e_a}}{N_{e_b}} m_{a,b}^f \quad (4)$$

281 with N_{e_a} being the effective population size of species a and N_{e_b} the one of species b . This approximation
282 becomes exact if the generation times of both species is the same, that is if $\frac{N_{e_a}}{N_{e_b}} = \frac{N_a}{N_b}$. In this manuscript, we
283 always use the forward in time definition of migration rates. Additional to sampling the rate itself, we sample the
284 probability of any migration rate to be 0 by using the BSSVS approach (Lemey et al., 2009b). By sampling any
285 rate being 0 or 1, we can estimate the support for gene flow between two species. Throughout this manuscript,
286 we assume the prior probability for gene flow between two species to be 5%.

287 Additionally to defining the rates, we implemented the possibility to define maximal rates of migration that
288 depend on the species tree directly. We implemented these in order to allow us to specify a maximal rate of gene
289 flow between two species where we expect that they are essentially not two species. To do so, we implemented
290 two different scenarios:

291 In the **overlap** scenario, we assume that the maximal backward in time rate of gene flow between two species
292 $m_{a,b}^{max}$ is inversely proportional to the time these species co-exist:

$$m_{a,b}^{max} = \frac{m_{tot}}{\min(t_{parent_A}, t_{parent_B}) - \max(t_A, t_B)} \quad (5)$$

293 with t_A denoting the node height of A and t_{parent_A} denoting the node height of the parent species of A . The
294 variable m_{tot} denotes an overall rate scaler that can be specified. This allows us to put maximal values on the
295 rate of gene flow that, while not exactly the same, are closely related to the percentage of lineages between
296 these two species to migrate.

297 In the **distance** scenario, we assume that any the maximal backward in time rate of gene flow between two
298 species $m_{a,b}^{max}$ is inversely proportional to the distance between the common ancestor :

$$m_{a,b} = \frac{m_{tot}}{t_{AB} - \max(t_A, t_B)} \quad (6)$$

299 with t_A denoting the node height of A and t_{parent_A} denoting the node height of the parent species of A . This
300 is to account for the maximal rate of gene flow being likely smaller between more distant species. Throughout
301 the manuscript, we used the overlap description of rates of gene flow.

302 The effective population sizes of extant and ancestral species are assumed to be log-normally distributed
303 with $\sigma = 0.25$. The mean of the log-normal distribution is estimated. Exact specifications for all parameters as
304 well as MCMC operators are provided in the BEAST2 xml input files here [https://github.com/nicfel/Isolation-](https://github.com/nicfel/Isolation-With-Migration)
305 [With-Migration](https://github.com/nicfel/Isolation-With-Migration).

306 Exploring different ranked species tree topologies

307 In order to operate on the species tree, we use the standard tree operators implemented in BEAST2. Gene flow
308 can only occur between co-existing species. The species which coexist changes when the rank (i.e ordering) of

309 speciation times or the topology of the species tree changes. When this occurs, we keep the rates of gene flow
310 between species that were co-existing before and after the operation the same. Rates of gene flow that disappear
311 during a move are randomly assigned to rates of gene flow between co-existing species that newly appear after
312 a move.

313 Summarizing posterior distributions of speciation histories

314 We implemented two ways to summarize a posterior distribution of species trees. In the first, we distinguish
315 between species trees with the different orderings of speciation events. To summarize the posterior distribution
316 of species trees, we first count the number of unique ranked tree topologies. For each unique ranked tree
317 topology, we then compute the distributions of rates of gene flow, effective population sizes and speciation
318 times. Alternatively, we summarize over posterior distributions of species trees, but ignore the ordering of
319 speciation times. In that case, we compute the distributions of rates of effective population sizes and speciation
320 times. For the rates of gene flow, we only consider those between species that are co-existing in all species trees
321 with the same topology, but potentially different ordering of speciation times.

322 Anopheles sequence data

323 We used the whole genome alignment (WGA) from Fontaine *et al.* (2015) (see also <https://doi.org/10.5061/dryad.f4114>)
324 for six species in the *An. gambiae* species complex: *An. gambiae* (AgamS1), *An. coluzzii*
325 (AcolM1), *An. arabiensis* (AaraD1), *An. melas* (AmelC2), *An. merus* (AmerM2), and *An. quadriannulatus*
326 (AquaS1), as well as two Pyrethophorus outgroup species (*An. christyi* (AchrA1) and *An. epiroticus* (AepiE1).
327 The *An. gambiae* PEST reference genome (AgamP4) was also included to anchor the chromosome assembled
328 coordinate system, but was not used for any other purpose, given this reference genome is a mixture of both
329 *An. gambiae* and *An. coluzzii*. In Fontaine *et al.* (2015), two WGA's were generated. Here we used the WGA
330 generated based on the reference assembly for each species using the MULTIZ feature from the Threaded
331 Blockset Aligner package v.12 (Blanchette *et al.*, 2004).

332 Based on the *AgamP4* PEST coordinate system, the WGA is partitioned into five chromosome arms: 2L,
333 2R, 3L, 3R, and X (the unplaced, draft Y, and mitogenome were not considered here). The AIM approach
334 assumes free recombination among loci, but no recombination within a locus. To meet those assumptions, we
335 subdivided the chromosome into loci of 1000 base pairs, a length small enough to minimize the probability that
336 recombination occurred within loci (Thawornwattana *et al.*, 2018). (Thawornwattana *et al.*, 2018) noticed that
337 local realignment was required to fix some misalignment in the original TBA WGA of Fontaine *et al.* (2015).
338 Thus we realigned all loci using MAFFT v.7.394 (Katoh and Standley 2013), using the iterative refinement
339 method (the L-INS-i option), following (Thawornwattana *et al.*, 2018). Only loci from the non-coding portion
340 of the genome were selected for further analyses, following the gross assumption that these loci would be closer
341 to neutrality than the coding regions.

342 We additionally removed loci that either badly aligned or were too divergent, which can also be a sign of
343 aligning badly. To do so, we only used loci in the analysis where at most 20% of all positions were gaps and at
344 most 40% of positions had nucleotide variations.

345 We assumed the genetic sequences to evolve according to an HKY+ Γ_4 model with a transition/transversion
346 rate that we estimated for each region individually, while fixing the base frequencies to the observed frequencies.
347 Additionally, we allowed each locus to have its own relative rate of evolution. Finally, we randomly subsampled
348 200 loci from the X chromosome and then jointly inferred the speciation history, gene flow, effective population
349 sizes and all evolutionary parameters. Additionally, we generated datasets with $\approx 5\%$ from the left arm of
350 chromosome 3, $\approx 5\%$ of the right arm of chromosome 3 and the rest from the X chromosome. We repeated
351 these step 3 times, in order to have 3 random subsets of loci and then ran each analyses using 2 different priors
352 on the migration rates. We additionally repeated all analysis using only 50 loci, as in Thawornwattana *et al.*
353 (2018), instead of 200 loci.

354 All the manipulations and processing of the WGA (in MAFF format) were conducted using Maffilter
355 1.3 (Dutheil et al., 2014).

356 **Software and Data Availability**

357 Simulation of gene trees given a species tree and migration rates were performed using the software MC-
358 coal in BPP (Yang, 2015b). Simulations of genetic sequences of length 1000 were performed using Seq-Gen
359 1.3.3 (Rambaut and Grassly, 1997), using a HKY site model with a transition/transversion ratio of 3 and base
360 frequency of 0.3,0.2,0.2 and 0.3. Data analyses were performed using BEAST 2.5 (Bouckaert et al., 2019). The
361 analysis of the *An. gambiae* species complex was performed using parallel tempering in the coupled MCMC
362 package (Mueller and Bouckaert, 2019). The source code of the BEAST2 package AIM can be downloaded
363 here: <https://github.com/genomescale/starbeast2>. All the scripts used in this study are publicly available at
364 <https://github.com/nicfel/Isolation-With-Migration>. Analyses were done using Matlab R2015b. Plotting was
365 done in R 3.2.3 using ggplot2 (Wickham, 2009). Trees were analysed by using ape 3.4 (Paradis et al., 2004)
366 and phytools 0.5-10 (Revell, 2012). A tutorial on how to set-up an AIM analysis can be found through the
367 <https://taming-the-beast.org/> platform (Barido-Sottani et al., 2017).

368 **Acknowledgement**

369 NM and TS were funded in part by the Swiss National Science foundation (SNF; grant number CR32I3_166258).
370 CZ is supported by the 100 Young Talents Program of Chinese Academy of Sciences and the Strategic Priority
371 Research Program of Chinese Academy of Sciences (XDB26000000). JEAR was supported by a PhD fellowship
372 from the GELIFES Adaptive Life program of the University of Groningen (The Netherlands).

373 References

- 374 Barido-Sottani, J., Bošková, V., Plessis, L. D., Kühnert, D., Magnus, C., Mitov, V., Müller, N. F., Pečerska, J., Rasmussen, D. A., Zhang,
375 C., *et al.* (2017). Taming the beast? a community teaching material resource for beast 2. *Systematic biology*, **67**(1), 170–174.
- 376 Blanchette, M., Kent, W. J., Riemer, C., Elnitski, L., Smit, A. F., Roskin, K. M., Baertsch, R., Rosenbloom, K., Clawson, H., Green, E. D.,
377 *et al.* (2004). Aligning multiple genomic sequences with the threaded blockset aligner. *Genome research*, **14**(4), 708–715.
- 378 Bouckaert, R., Heled, J., Kühnert, D., Vaughan, T., Wu, C.-H., Xie, D., Suchard, M. A., Rambaut, A., and Drummond, A. J. (2014).
379 BEAST 2: a software platform for Bayesian evolutionary analysis. *PLoS Computational Biology*, **10**(4), e1003537.
- 380 Bouckaert, R., Vaughan, T. G., Barido-Sottani, J., Duchêne, S., Fourment, M., Gavryushkina, A., Heled, J., Jones, G., Kühnert, D.,
381 De Maio, N., *et al.* (2019). Beast 2.5: An advanced software platform for bayesian evolutionary analysis. *PLoS computational biology*,
382 **15**(4), e1006650.
- 383 Clark, A. G. and Messer, P. W. (2015). Conundrum of jumbled mosquito genomes. *Science*, **347**(6217), 27–28.
- 384 Davidson, G. (1962). Anopheles gambiae complex. *Nature*, **196**(4857), 907.
- 385 De Maio, N., Wu, C.-H., O'Reilly, K. M., and Wilson, D. (2015). New Routes to Phylogeography: A Bayesian Structured Coalescent
386 Approximation. *PLoS genetics*, **11**(8), e1005421.
- 387 Dutheil, J. Y., Gaillard, S., and Stukenbrock, E. H. (2014). Maffilter: a highly flexible and extensible multiple genome alignment files
388 processor. *BMC genomics*, **15**(1), 53.
- 389 Flot, J.-F. (2010). Seqphase: a web tool for interconverting phase input/output files and fasta sequence alignments. *Molecular Ecology*
390 *Resources*, **10**(1), 162–166.
- 391 Fontaine, M. C., Pease, J. B., Steele, A., Waterhouse, R. M., Neafsey, D. E., Sharakhov, I. V., Jiang, X., Hall, A. B., Catteruccia, F.,
392 Kakani, E., Mitchell, S. N., Wu, Y.-C., Smith, H. A., Love, R. R., Lawniczak, M. K., Slotman, M. A., Emrich, S. J., Hahn, M. W., and
393 Besansky, N. J. (2015). Extensive introgression in a malaria vector species complex revealed by phylogenomics. *Science*, **347**(6217),
394 1258524.
- 395 Heled, J. and Drummond, A. J. (2010). Bayesian inference of species trees from multilocus data. *Molecular Biology and Evolution*, **27**(3),
396 570–580.
- 397 Hey, J. (2009). The divergence of chimpanzee species and subspecies as revealed in multipopulation isolation-with-migration analyses.
398 *Molecular biology and evolution*, **27**(4), 921–933.
- 399 Hey, J. (2010). Isolation with migration models for more than two populations. *Molecular Biology and Evolution*, **27**(4), 905–920.
- 400 Hey, J. and Nielsen, R. (2004). Multilocus methods for estimating population sizes, migration rates and divergence time, with applications
401 to the divergence of *Drosophila pseudoobscura* and *D. persimilis*. *Genetics*, **167**(2), 747–760.
- 402 Hey, J. and Nielsen, R. (2007). Integration within the Felsenstein equation for improved Markov chain Monte Carlo methods in population
403 genetics. *Proceedings of the National Academy of Sciences of the United States of America*, **104**(8), 2785–2790.
- 404 Hey, J., Chung, Y., Sethuraman, A., Lachance, J., Tishkoff, S., Sousa, V. C., and Wang, Y. (2018). Phylogeny estimation by integration
405 over isolation with migration models. *Molecular biology and evolution*, **35**(11), 2805–2818.
- 406 Kaessmann, H., Wiebe, V., and Pääbo, S. (1999). Extensive nuclear dna sequence diversity among chimpanzees. *Science*, **286**(5442),
407 1159–1162.
- 408 Keightley, P. D., Ness, R. W., Halligan, D. L., and Haddrill, P. R. (2014). Estimation of the spontaneous mutation rate per nucleotide site
409 in a drosophila melanogaster full-sib family. *Genetics*, **196**(1), 313–320.
- 410 Leaché, A. D., Harris, R. B., Rannala, B., and Yang, Z. (2014). The influence of gene flow on species tree estimation: a simulation study.
411 *Systematic Biology*, **63**(1), 17–30.
- 412 Lemey, P., Rambaut, A., Drummond, A. J., and Suchard, M. a. (2009a). Bayesian phylogeography finds its roots. *PLoS Computational*
413 *Biology*, **5**(9), e1000520.
- 414 Lemey, P., Rambaut, A., Drummond, A. J., and Suchard, M. A. (2009b). Bayesian phylogeography finds its roots. *PLoS computational*
415 *biology*, **5**(9), e1000520.
- 416 Lemey, P., Rambaut, A., Bedford, T., Faria, N., Bielejec, F., Baele, G., Russell, C. A., Smith, D. J., Pybus, O. G., Brockmann, D., *et al.*
417 (2014). Unifying viral genetics and human transportation data to predict the global transmission dynamics of human influenza h3n2.
418 *PLoS pathogens*, **10**(2), e1003932.

- 419 Liu, L., Yu, L., Kubatko, L., Pearl, D. K., and Edwards, S. V. (2009). Coalescent methods for estimating phylogenetic trees. Molecular
420 Phylogenetics and Evolution, **53**(1), 320–328.
- 421 Mallet, J., Besansky, N., and Hahn, M. W. (2016). How reticulated are species? BioEssays, **38**(2), 140–149.
- 422 Mueller, N. F. and Bouckaert, R. (2019). Coupled mcmc in beast 2. bioRxiv, page 603514.
- 423 Mueller, N. F., Dudas, G., and Stadler, T. (2018). Inferring time-dependent migration and coalescence patterns from genetic sequence and
424 predictor data in structured populations. bioRxiv, page 342329.
- 425 Müller, N. F., Rasmussen, D. A., and Stadler, T. (2017). The structured coalescent and its approximations. Molecular biology and evolution,
426 **34**(11), 2970–2981.
- 427 Müller, N. F., Rasmussen, D., and Stadler, T. (2018). Mascot: parameter and state inference under the marginal structured coalescent
428 approximation. Bioinformatics, **34**(22), 3843–3848.
- 429 Nielsen, R. and Wakeley, J. (2001). Distinguishing migration from isolation: a Markov chain Monte Carlo approach. Genetics, **158**(2),
430 885–896.
- 431 Ogilvie, H. A., Bouckaert, R. R., and Drummond, A. J. (2017). StarBEAST2 brings faster species tree inference and accurate estimates of
432 substitution rates. Molecular Biology and Evolution.
- 433 Ogilvie, H. A., Vaughan, T. G., Matzke, N. J., Slater, G. J., Stadler, T., Welch, D., and Drummond, A. J. (2018). Inferring species trees
434 using integrative models of species evolution. bioRxiv, page 242875.
- 435 Paradis, E., Claude, J., and Strimmer, K. (2004). APE: Analyses of Phylogenetics and Evolution in R language. Bioinformatics (Oxford,
436 England), **20**(2), 289–90.
- 437 Prado-Martinez, J., Sudmant, P. H., Kidd, J. M., Li, H., Kelley, J. L., Lorente-Galdos, B., Veeramah, K. R., Woerner, A. E., O'Connor,
438 T. D., Santpere, G., et al. (2013). Great ape genetic diversity and population history. Nature, **499**(7459), 471.
- 439 Rambaut, A. and Grassly, N. C. (1997). Seq-Gen: an application for the Monte Carlo simulation of DNA sequence evolution along
440 phylogenetic trees. Computer Applications in the Biosciences : CABIOS, **13**(3), 235–238.
- 441 Rannala, B. and Yang, Z. (2003). Bayes estimation of species divergence times and ancestral population sizes using DNA sequences from
442 multiple loci. Genetics, **164**(4), 1645–1656.
- 443 Revell, L. J. (2012). phytools: an R package for phylogenetic comparative biology (and other things). Methods in Ecology and Evolution,
444 **3**(2), 217–223.
- 445 Sousa, V. and Hey, J. (2013). Understanding the origin of species with genome-scale data: modelling gene flow. Nature Reviews Genetics,
446 **14**(6), 404–414.
- 447 Stadler, T. (2010). Sampling-through-time in birth–death trees. Journal of theoretical biology, **267**(3), 396–404.
- 448 Stephens, M. and Scheet, P. (2005). Accounting for decay of linkage disequilibrium in haplotype inference and missing-data imputation.
449 The American Journal of Human Genetics, **76**(3), 449–462.
- 450 Thawornwattana, Y., Dalquen, D., and Yang, Z. (2018). Coalescent analysis of phylogenomic data confidently resolves the species relation-
451 ships in the anopheles gambiae species complex. Molecular Biology and Evolution, **35**(10), 2512–2527.
- 452 White, B. J., Collins, F. H., and Besansky, N. J. (2011). Evolution of anopheles gambiae in relation to humans and malaria. Annual review
453 of ecology, evolution, and systematics, **42**, 111–132.
- 454 Wickham, H. (2009). ggplot2: Elegant Graphics for Data Analysis. Springer-Verlag New York.
- 455 Wilkinson-Herbots, H. M. (2008). The distribution of the coalescence time and the number of pairwise nucleotide differences in the "isolation
456 with migration" model. Theoretical Population Biology, **73**(2), 277–288.
- 457 Wilkinson-Herbots, H. M. (2012). The distribution of the coalescence time and the number of pairwise nucleotide differences in a model of
458 population divergence or speciation with an initial period of gene flow. Theoretical Population Biology, **82**(2), 92–108.
- 459 Yang, Z. (2015a). The bpp program for species tree estimation and species delimitation. Current Zoology, **61**(5), 854–865.
- 460 Yang, Z. (2015b). The BPP program for species tree estimation and species delimitation. Current Zoology, **61**(5), 854–865.
- 461 Yu, N., Chen, F.-C., Ota, S., Jorde, L. B., Pamilo, P., Patthy, L., Ramsay, M., Jenkins, T., Shyue, S.-K., and Li, W.-H. (2002). Larger
462 genetic differences within africans than between africans and eurasiens. Genetics, **161**(1), 269–274.

- 463 Yu, N., Jensen-Seaman, M. I., Chemnick, L., Kidd, J. R., Deinard, A. S., Ryder, O., Kidd, K. K., and Li, W.-H. (2003). Low nucleotide
464 diversity in chimpanzees and bonobos. Genetics, **164**(4), 1511–1518.
- 465 Yu, N., Jensen-Seaman, M. I., Chemnick, L., Ryder, O., and Li, W.-H. (2004). Nucleotide diversity in gorillas. Genetics, **166**(3), 1375–1383.
- 466 Yule, G. U. (1925). A mathematical theory of evolution, based on the conclusions of dr. j. c. willis, fr s. Philosophical transactions of the
467 Royal Society of London. Series B, containing papers of a biological character, **213**(402-410), 21–87.

468 **Supplementary Material**

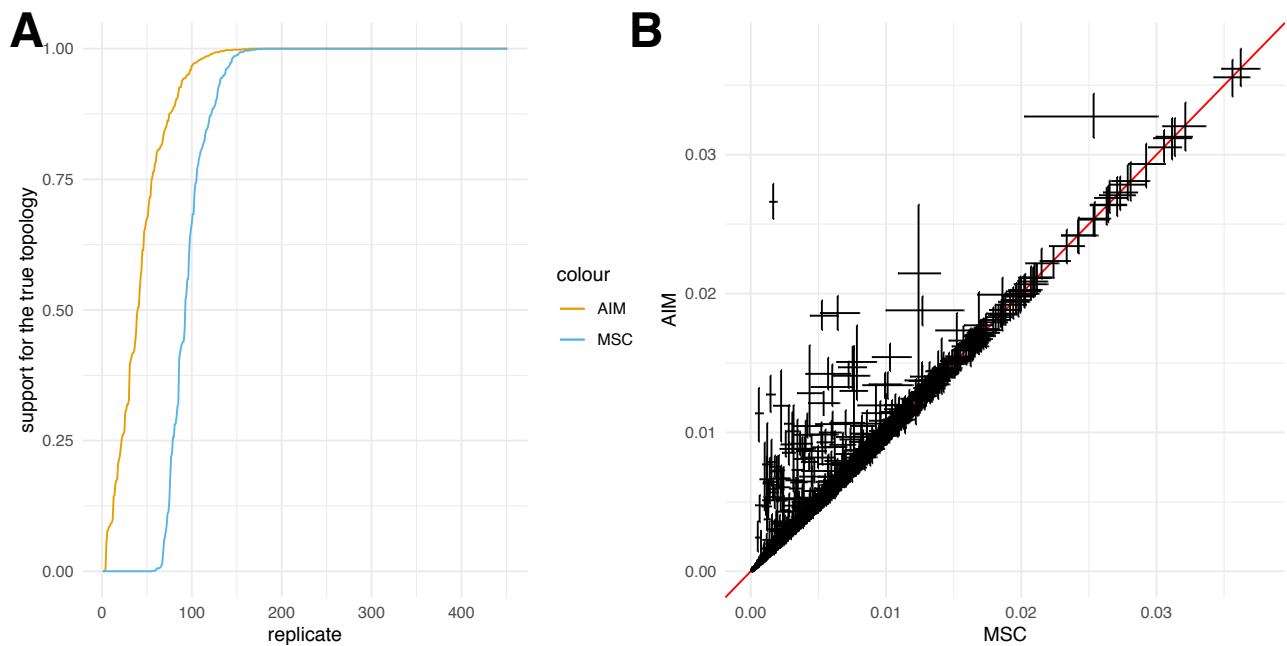


Figure S1: **Comparison of species tree and speciation time inference using AIM and MSC.** **A** Posterior support for the true species tree topology inferred using the approximate isolation with migration (AIM) model and the multispecies coalescent (MSC) **B** Comparison between the 95% highest posterior density intervals of speciation times between AIM and MSC. As shown in figure 1C, AIM infers the true speciation times well. The multispecies coalescent either correctly infers speciation times or underestimates them.

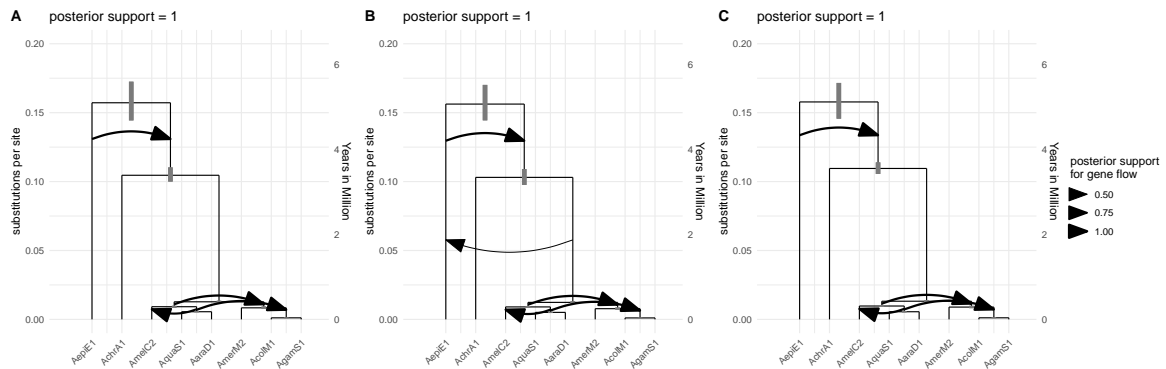


Figure S2: **Inferred species histories with gene flow for 3 random subsets of 200 loci from the X-chromosome.** Inferred species history for all 8 anopheles species including the two outgroups *An. christyi* and *An. epiroticus*, with support for ancestral gene flow between them. The 3 different trees show the results for 3 different subsets of 200 loci randomly sampled from the X-Chromosome. The node heights are the median inferred speciation times. The grey bars show the 95% highest posterior density intervals for speciation times. The heights are given in substitutions per site. The cutoff for an arrow to be plotted is a posterior support for gene flow of at least 0.5.

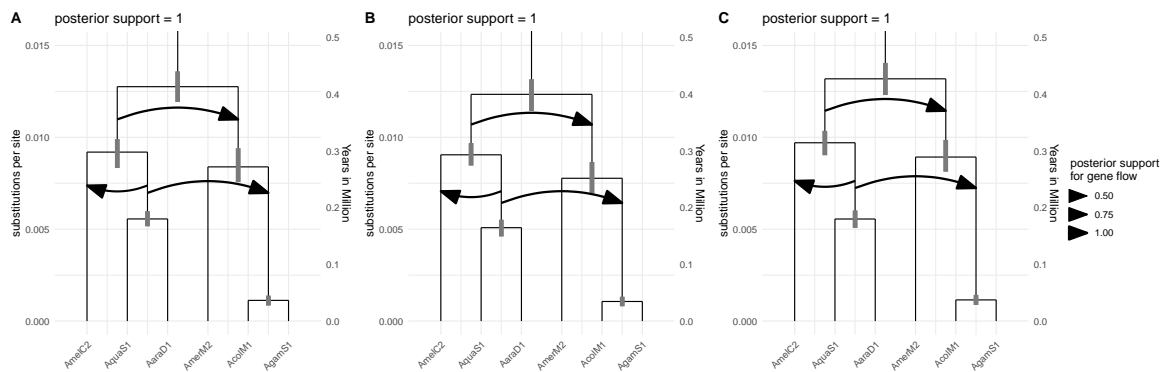


Figure S3: **Inferred species histories with gene flow for 3 random subsets of 200 loci from the X-chromosome zooming in into the *An. gambiae* species complex.** Inferred species history for all 6 anopheles species without the two outgroups *An. christyi* and *An. epiroticus*. The node heights are the median inferred speciation times. The grey bars show the 95% highest posterior density intervals for speciation times. The heights are given in substitutions per site. The cutoff for an arrow to be plotted is a posterior support for gene flow of at least 0.5.

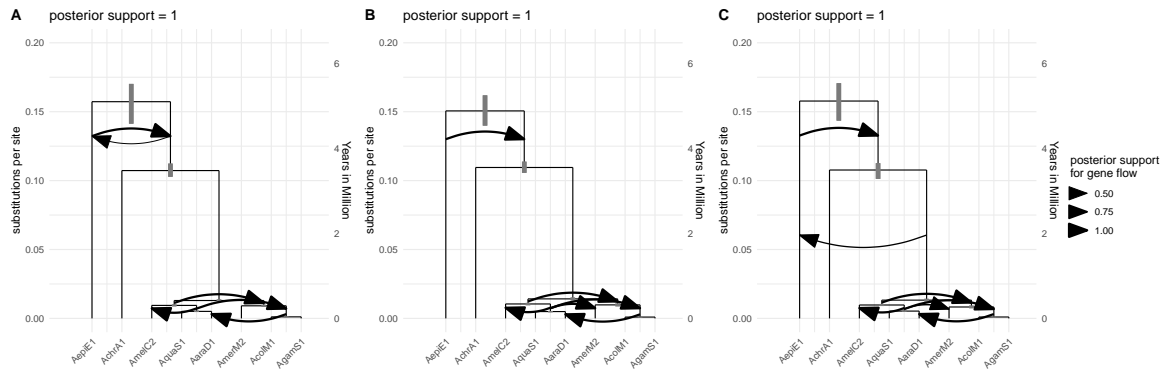


Figure S4: **Inferred species histories with gene flow for 3 random subsets of 200 loci from the X chromosome and chromosome 3.** Inferred species history for all 8 anopheles species including the two outgroups *An. christyi* and *An. epiroticus*, with support for ancestral gene flow between them. The 3 different trees show the results for 3 different subsets of 200 loci randomly sampled from the X chromosome (with probability 0.9) and chromosome 3 (with probability 0.1). The node heights are the median inferred speciation times. The grey bars show the 95% highest posterior density intervals for speciation times. The heights are given in substitutions per site. The cutoff for an arrow to be plotted is a posterior support for gene flow of at least 0.5.

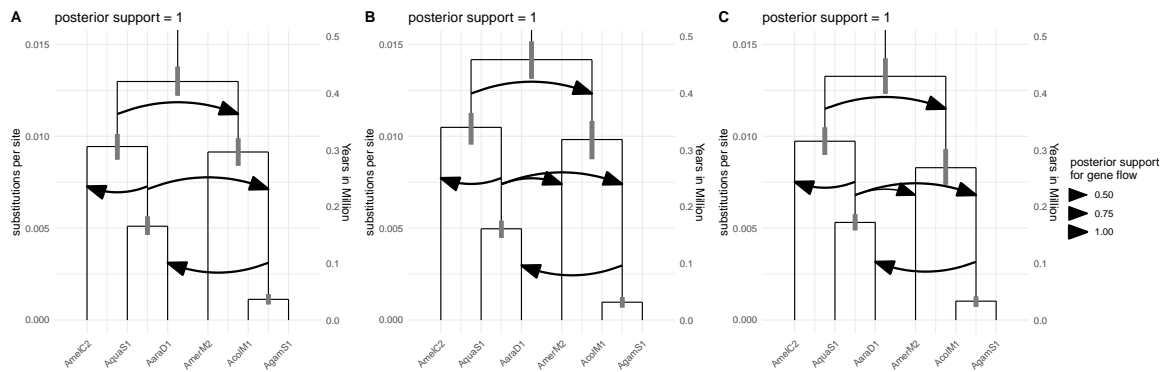


Figure S5: **Inferred species histories with gene flow for 3 random subsets of 200 loci from the X-chromosome zooming in into the *An. gambia* species complex.** Inferred species history for all 6 anopheles species without the two outgroups *An. christyi* and *An. epiroticus*. The node heights are the median inferred speciation times. The grey bars show the 95% highest posterior density intervals for speciation times. The heights are given in substitutions per site. The cutoff for an arrow to be plotted is a posterior support for gene flow of at least 0.5.